International Journal of Solids and Structures 49 (2012) 3416–3421

Contents lists available at SciVerse ScienceDirect

International Journal of Solids and Structures

journal homepage: www.elsevier.com/locate/ijsolstr

# Mechanics of stretchable electronics with high fill factors

Yewang Su [a,b], Zhuangjian Liu [c], Seok Kim [d], Jian Wu [b,e], Yonggang Huang [a,*], John A. Rogers [d,f,*]

[a] Depts. of Civil/Environ. Eng. & Mechanical Eng., Northwestern University, Evanston, IL 60208, United States
[b] Center for Mechanics and Materials, Tsinghua University, Beijing 100084, China
[c] Institute of High Performance Computing, A*STAR 138632, Singapore
[d] Department of Mechanical Science and Engineering, University of Illinois, Urbana, IL 61801, United States
[e] Department of Engineering Mechanics, Tsinghua University, Beijing 100084, China
[f] Depts. of Material Sci. & Eng., Electrical & Computer Eng., Chemistry, Materials Research Lab., and Beckman Institute, University of Illinois, Urbana, IL 61801, United States

ARTICLE INFO

*Article history:*
Received 1 December 2011
Received in revised form 23 June 2012
Available online 7 August 2012

*Keywords:*
Self collapse
Stretchable electronics
Transfer printing
Biomimetics
Stretchability and bendability

ABSTRACT

Mechanics models are developed for an imbricate scale design for stretchable and flexible electronics to achieve both mechanical stretchability and high fill factors (e.g., full, 100% areal coverage). The critical conditions for self collapse of scales and scale contact give analytically the maximum and minimum widths of scales, which are important to the scale design. The maximum strain in scales is obtained analytically, and has a simple upper bound of $3t_{scale}/(4\rho)$ in terms of the scale thickness $t_{scale}$ and bending radius $\rho$.



## 1. Introduction

Stretchable and flexible electronics have performance equal to established technologies that use rigid semiconductor wafers, but have mechanical properties of a rubber band (Rogers et al., 2010). They enable many new application possibilities, such as structural health monitoring devices (Nathan et al., 2000), flexible sensors (Lumelsky et al., 2001; Mannsfeld et al., 2010; Someya et al., 2005; Someya and Sekitani, 2009), smart surgical gloves (Someya et al., 2004), flexible display (Crawford, 2005; Forrest, 2004; Gelinck et al., 2004); electronic eye camera (Jin et al., 2004; Ko et al., 2008); stretchable and foldable circuits (Kim et al., 2008a; Sekitani et al., 2010), and flexible solar cell (Yoon et al., 2008) and LED (Park et al., 2009; Sekitani et al., 2009). Stretchable and flexible electronics have recently been applied to medicine, such as to cardiac electrophysiology (Viventi et al., 2010), bio-integrated electronics (Kim et al., 2010a), water-proof optoelectronics for biomedicine (Kim et al., 2010b), advanced catheter technology (Kim et al., 2011a), epidermal electronics (Kim et al., 2011b), and flexible and foldable surface electrodes for measuring brain activity (Viventi et al., 2011).

Fig. 1a shows the mesh design of stretchable and flexible electronics (Kim et al., 2008b; Song et al., 2009; Su et al., 2012). The device islands connected by interconnect bridges are structured into a mesh and bond to a pre-stretched elastomeric substrate of PDMS only at the islands. Release of pre-stretch in the substrate leads to buckling of bridges to form arc-shaped bridge structures (Fig. 1b) that can move freely out of the plane to accommodate large applied strains (e.g., >100%), even to values that approach the fracture limits of the PDMS. Serpentine interconnect bridges have also been used to reach even higher stretchability (Kim et al., 2008b).

The island-bridge design in Fig. 1, however, reduces the fill factor (number of devices per unit area) of stretchable electronics since the area outside the device islands is not effectively used. Kim et al. (2012) proposed an imbricate scale design that can provide mechanical stretchability and high fill factor (e.g., full, 100% areal coverage). As illustrated in Fig. 2, scales (rigid plates on which electronics are fabricated) were transfer printed from a donor substrate onto a PDMS backing layer with molded posts. A stamp with microtips at corners was first pressed with high preload against a scale on a donor substrate, which led to mechanical collapse of the stamp and therefore large stamp/scale contact region between microtips. The stamp was then rapidly retracted to lift the scale from the donor. Shortly afterward the compressed microtips relaxed back to their original shape due to restoring forces in PDMS, leaving small stamp/scale contact region only at the microtips. The scale was then gently placed on a post of the PDMS backing layer,

* Corresponding authors. Addresses: Depts. of Civil/Environ. Eng. & Mechanical Eng., Northwestern University, Evanston, IL 60208, United States (Y. Huang). Dept. of Material Sci. & Eng., University of Illinois, Urbana, IL 61801, United States (J.A. Rogers). Tel.: +1 217 265 5072; fax: +1 217 244 6534 (Y. Huang).

*E-mail addresses:* y-huang@northwestern.edu (Y. Huang), jrogers@illinois.edu (J.A. Rogers).

0020-7683/$ - see front matter Crown Copyright © 2012 Published by Elsevier Ltd. All rights reserved.
http://dx.doi.org/10.1016/j.ijsolstr.2012.07.024

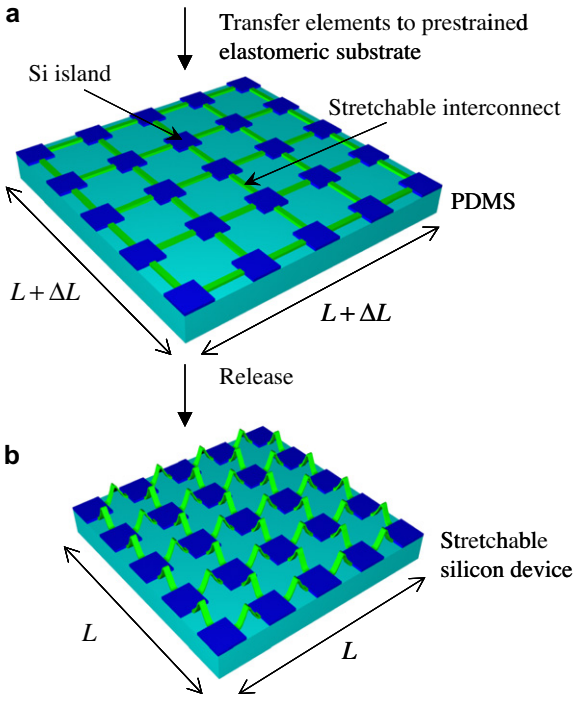


**Fig. 1.** Schematic illustration of fabrication process for stretchable electronics with the noncoplanar mesh design on a compliant substrate; (a) mesh on a pre-stretched substrate; and (b) buckled mesh after the release of pre-stretch in the substrate. (Copyright 2009 American Institute of Physics.)

followed by slow retraction of the stamp. The scale/post bonding was accomplished using surface hydroxyl condensation reactions. The lateral dimensions of scales (600 × 600 μm) exceeded the post spacing (500 μm), which yielded imbricate layouts with overlaps (of 100 μm) for adjacent scales, as illustrated in Fig. 3a and b. The overlaps changed in size during deformation, but they never disappeared, which enabled full, 100% effective area coverage, i.e., reaching the maximal fill factor of one.

Mechanics models for imbricate scales are established in this paper. An important design consideration is to prevent the scales from self collapsing onto the PDMS backing layer due to scale/PDMS adhesion. A simple, analytical expression for the maximum width of scale is obtained in Section 2. Section 3 gives analytically the maximum stretchability and bendability of scales that still remain in contact during deformation. The maximum strain in scales is obtained in Section 4 via both analytical model and finite element method.

## 2. Self collapse of the scale onto PDMS backing layer

Fig. 4 illustrates self collapse of a scale onto the PDMS backing layer due to scale/PDMS adhesion. For simplicity the scale is modeled as a beam with the bending stiffness $\overline{EI}_{scale}$, width $w_{scale}$, and thickness $t_{scale}$. The post width and thickness are denoted by $w_{post}$ and $t_{post}$, respectively. Deformation of the post is negligible, as to be shown at the end of this section. The PDMS backing layer is much thicker than the scale and post.

Let $y$ denote the deflection of scale over the part $L$ (Fig. 4) that does not contact the post and backing layer. Only the right half of scale is analyzed due to symmetry. The equilibrium equation of the beam gives $\overline{EI}_{scale} d^4y/dx^4 = 0$, where $x$ is the coordinate with origin at the top right corner of the post. The boundary conditions are $y|_{x=0} = 0$, $y|_{x=L} = -t_{post}$, and $y'|_{x=0} = y'|_{x=L} = 0$. This gives the deflection

$$y = t_{post}\left[2\left(\frac{x}{L}\right)^3 - 3\left(\frac{x}{L}\right)^2\right]. \tag{1}$$

The bending energy in the beam is $\int_0^L (\overline{EI}_{scale}/2) y''^2 dx = 6\overline{EI}_{scale} t_{post}^2/L^3$. The total energy is

$$U = \frac{6\overline{EI}_{scale}}{L^3} t_{post}^2 - \gamma\left(\frac{w_{scale} - w_{post}}{2} - L\right), \tag{2}$$

where $\gamma$ and $(w_{scale} - w_{post})/2 - L$ are the work of adhesion and contact length between the scale and PDMS backing layer, respectively. Minimization of energy $\partial U/\partial L = 0$ gives

$$L = \left(\frac{18\overline{EI}_{scale}}{\gamma} t_{post}^2\right)^{1/4}. \tag{3}$$

The total energy is obtained by substituting Eq. (3) into Eq. (2), which must be larger than the energy without collapse (i.e., zero) to prevent self collapse of the scale. This gives the maximum width of scale as

$$w_{scale} \leqslant w_{post} + 8\left(\frac{2\overline{EI}_{scale} t_{post}^2}{9\gamma}\right)^{1/4} \tag{4}$$

to prevent self collapse of the scale. For $\overline{EI}_{scale} = \overline{E}_{scale} t_{scale}^3/12$ with $\overline{E}_{scale} = 140$ GPa and $t_{scale} = 3$ μm, $w_{post} = 140$ μm, $t_{post} = 80$ μm, and $\gamma = 0.15$ Jm$^{-2}$ in experiments (Kim et al., 2012), the above equation gives $w_{scale} \leqslant 2.01$ mm. The scale width in experiments $w_{scale} = 600$ μm, at which no self collapse is observed, indeed satisfies this condition.

The change of post thickness due to self collapse of the scale can be estimated the compression due to the scale/post contact force

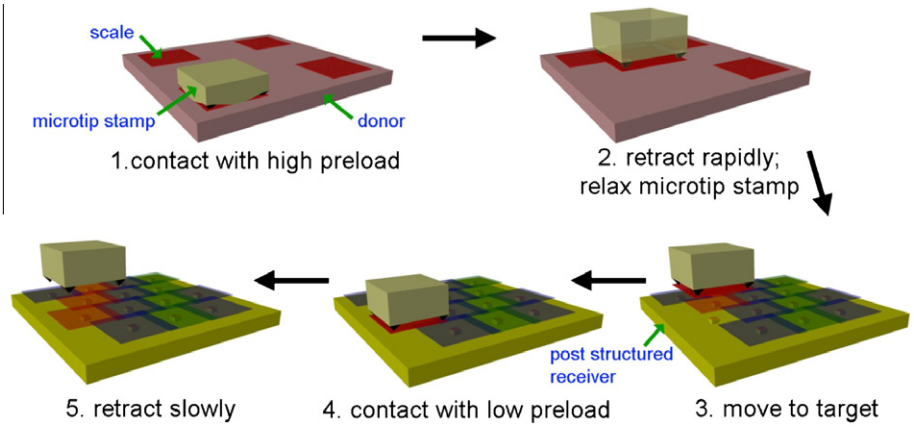


**Fig. 2.** Schematic illustration of fabrication process for stretchable electronics with an imbricate scale design on a compliant backing layer.

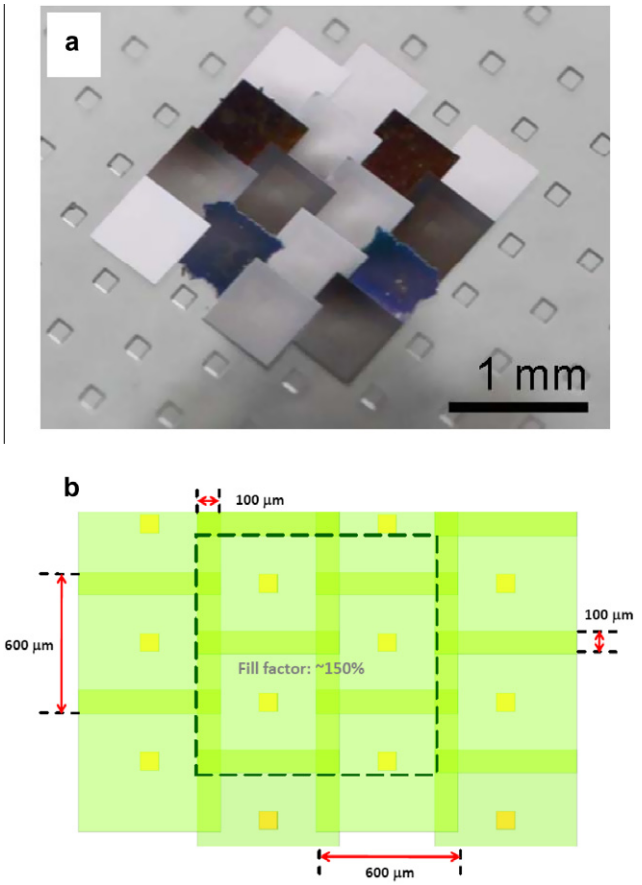


**Fig. 3.** (a) Optical image of scales with posts on the PDMS backing layer; and (b) schematic illustration of the scales, posts and their spacing.

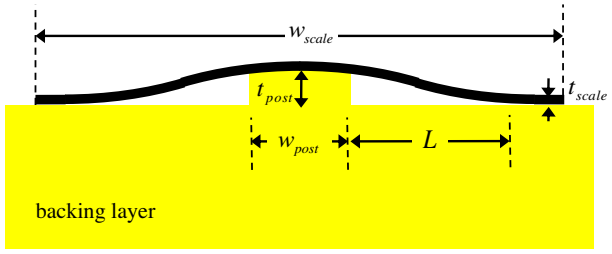


**Fig. 4.** Schematic illustration of self collapse of a scale on a backing layer.

as $4[(2/9)\overline{EI}_{scale}\gamma^3 t_{post}^2]^{1/4}/(E_{post}w_{post})$. It is 0.56 μm for the PDMS post ($E_{post}$ = 1.8 MPa) and other parameters given above, which is much smaller than the post thickness $t_{post}$ = 80 μm and is therefore negligible.

## 3. Stretchability and bendability

As illustrated in Fig. 5, the stretchability and bendability is reached when the overlap between neighbor scales vanishes, which is also the limit for reversible deformation of the scales. Let $t_{backinglayer}$ denote the backing layer thickness, $s_{post}$ the center-to-center post spacing, and $\varepsilon_{applied}$ and $\rho$ the tensile strain and bending radius applied to the backing layer, respectively. The post spacing (at the mid-plane) changes to $(1+\varepsilon_{applied})s_{post}$ after stretching, which gives the angle between two posts $\theta = (1+\varepsilon_{applied})s_{post}/\rho$. The bending radius at the scale center is $\rho + t_{post} + (t_{backinglayer}/2)$.

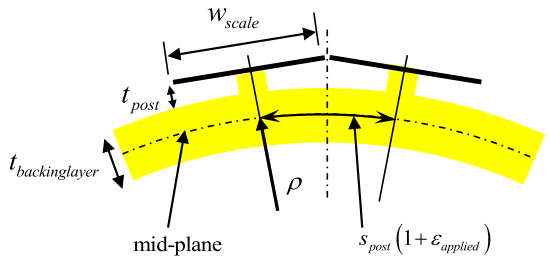


**Fig. 5.** Schematic illustration of the critical state when neighbor scales start to separate after stretching and bending.

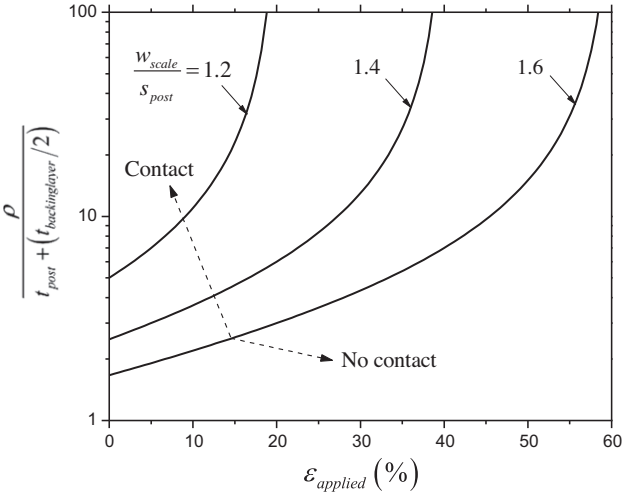


**Fig. 6.** The normalized bending radius, $\rho/[t_{post} + (t_{backinglayer}/2)]$, versus the applied strain $\varepsilon_{applied}$ for several ratios of scale width $w_{scale}$ to post spacing $s_{post}$ at the critical state when neighbor scales start to separate, where $t_{post}$ and $t_{backinglayer}$ are the thicknesses of the post and backing layer, respectively.

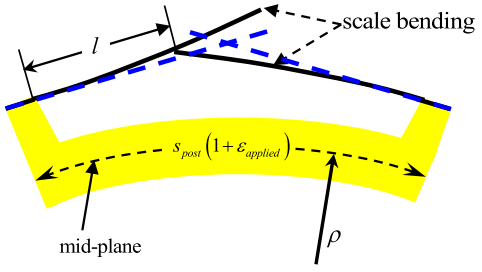


**Fig. 7.** Schematic illustration of scale bending induced by contact between neighbor scales.

For scales to remain in imbricate configurations, the minimal scale width is given by

$$w_{scale} \geqslant (2\rho + 2t_{post} + t_{backinglayer}) \tan\left[\frac{s_{post}}{2\rho}(1+\varepsilon_{applied})\right]. \quad (5)$$

For $w_{scale}$ = 600 μm, $t_{post}$ = 80 μm, $s_{post}$ = 500 μm and $t_{backinglayer}$ = 800 μm in experiments (Kim et al., 2012), the minimal bending radius is 2.45 mm without the applied strain, and increases to 5.35 mm for applied strain $\varepsilon_{applied}$ = 10%. The bending radius in experiments $\rho$ = 17 mm, at which the scales remain in contact, is indeed larger than these minimal values.

For the bending radius much larger than the post spacing and thickness and backing layer thickness, i.e., $\rho \gg s_{post}, 2t_{post} + t_{backinglayer}$, Eq. (5) can be simplified to

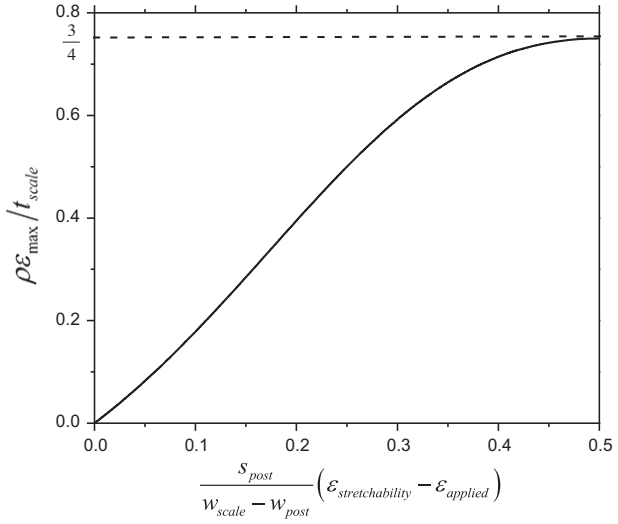


**Fig. 8.** The normalized maximum strain, $\rho\varepsilon_{\max}/t_{scale}$, versus $(\varepsilon_{stretchability}-\varepsilon_{applied})$ $s_{post}/(w_{scale}-w_{post})$, where $\rho$ is the bending radius, $\varepsilon_{applied}$ is the applied strain, $\varepsilon_{stretchability}$ is the stretchability, $w_{scale}$, $t_{scale}$, $w_{post}$ and $s_{post}$ are the scale width and thickness, and post width and spacing, respectively.

$$(1+\varepsilon_{applied})\left(1+\frac{t_{post}+\frac{1}{2}t_{backinglayer}}{\rho}\right)\leqslant\frac{w_{scale}}{s_{post}}. \tag{6}$$

Fig. 6 shows the normalized minimal bending radius, $\rho/[t_{post}+(t_{backinglayer}/2)]$, above which the neighbor scales remain in contact, versus the applied strain $\varepsilon_{applied}$, for several ratios of scale width to post spacing, $w_{scale}/s_{post}$. The maximum stretchability is obtained analytically as $\varepsilon_{stretchability}=(w_{scale}/s_{post})-1$ (when $\rho\to\infty$). The minimal bending radius without the applied strain is also obtained analytically as $[t_{post}+(t_{backinglayer}/2)][(w_{scale}/s_{post})-1]^{-1}$.

It should be pointed out that the deformation of scales is fully reversible because Eq. (5) [or Eq. (6)] ensures that the neighboring scales remain contact. The above analysis holds for both convex (Fig. 5) and concave bending (i.e., bending opposite to that in Fig. 5) except that the bending radius $\rho$ is negative for the latter. For concave bending, the scales touch the substrate when the bending radius reaches $\rho=-[w_{scale}^2/(4t_{post})+t_{post}+t_{backinglayer}]/2$.

## 4. Maximum strain in the scale

Fig. 7 shows the deformed scales subject to the bending radius $\rho$ and applied strain $\varepsilon_{applied}$. The left and right scales contact a point, which has the distances $l$ (to be determined) and $(w_{scale}-w_{post})/2$ to the clamped ends of the left and right scales, respectively. The normal force $P$ at the contact point between two scales is to be determined. Deflections of the left and right scales are obtained in terms of $l$ and $P$ via the beam theory (Gere and Timoshenko, 2003). Continuity of displacements at the contact point, accounting for the rotation at the clamped ends due to relatively large bending radius $\rho\gg s_{post}$, $t_{post}+(t_{backinglayer}/2)$, gives $l$ and $P$ as

$$l=(1+\varepsilon_{applied})s_{post}-\frac{1}{2}(w_{scale}+w_{post}), \tag{7}$$

$$P=\frac{6\overline{EI}_{scale}}{s_{post}\rho}\times\frac{\varepsilon_{stretchability}-\varepsilon_{applied}}{3(\varepsilon_{stretchability}-\varepsilon_{applied})^2+\left(\varepsilon_{stretchability}-\varepsilon_{applied}-\frac{w_{scale}-w_{post}}{s_{post}}\right)^2}, \tag{8}$$

where the maximum stretchability $\varepsilon_{stretchability}=(w_{scale}/s_{post})-1$ is obtained in Section 3, at which the contact force $P$ vanishes.

The maximum strain in scales is reached at the clamped end of the right scale since it is longer than the left one. It is obtained from the beam theory as

$$\varepsilon_{\max}=\frac{t_{scale}}{2\rho}\frac{\eta}{\eta^2+\frac{1}{3}(\eta-1)^2}, \tag{9}$$

where $\eta=(\varepsilon_{stretchability}-\varepsilon_{applied})s_{post}/(w_{scale}-w_{post})$. The maximum strain is linearly proportional to the ratio of scale thickness to bending radius, $t_{scale}/\rho$, and also depends on the applied strain $\varepsilon_{applied}$, scale width $w_{scale}$, and post width $w_{post}$ and spacing $s_{post}$ via a single dimensionless parameter $\eta$. Fig. 8 shows the normalized maximum strain $\rho\varepsilon_{\max}/t_{scale}$ versus $\eta$. The curve has a maximum 3/4 such that an upper bound estimate of the maximum strain in the scales is

$$\varepsilon_{\max}=\frac{3t_{scale}}{4\rho}. \tag{10}$$

For the bending radius ρ = 17 mm, applied strain εapplied = 0, and tscale = 3 μm, wscale = 600 μm, wpost = 140 μm and spost = 500 μm

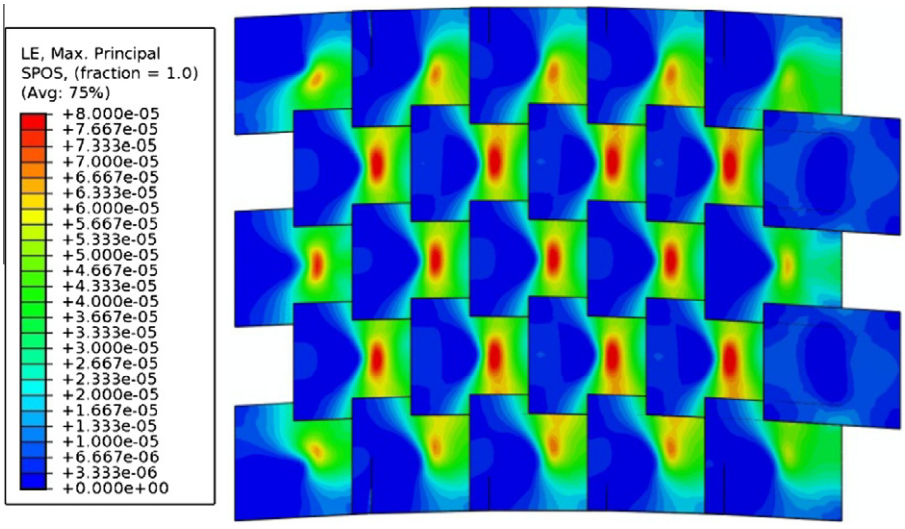


**Fig. 9.** The distribution of maximum principal strain in scales obtained by the finite element method for scales on a PDMS substrate with posts, bent to a 17 mm radius of curvature.

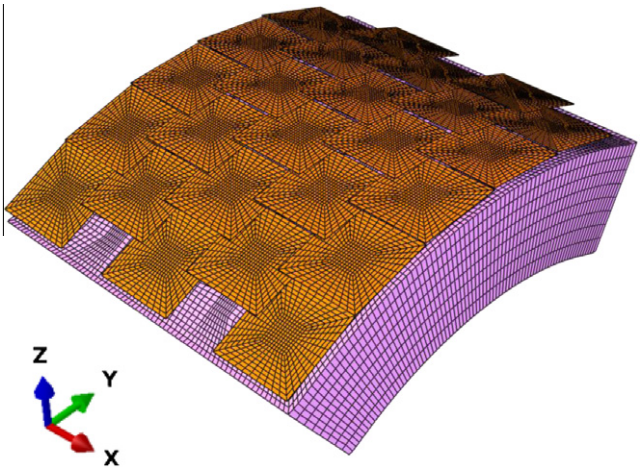


**Fig. 10.** The deformed mesh of scales and substrate.

in experiments, the maximum strain in Eq. (9) is 0.0076%. This agrees well with the maximum strain 0.008% obtained by the finite element analysis (FEA) shown in Fig. 9, which gives the distribution of maximum principal strain in scales. The 8-node, hexahedral brick element C3D8R and 8-node, quadrilateral in-plane general-purpose continuum shell element SC8R in the FEA package ABAQUS are used for the backing layer and scales, respectively. The total number of elements exceeds 80,000. The scales are bonded to the posts, and the scales contact without friction. Fig. 10 shows the deformed mesh in FEA.

## 5. Concluding remarks

Mechanics models are established for the imbricate design of stretchable electronics to achieve high fill factors (complete areal coverage).

(1) Eq. (4) based on the condition for self collapse of scales onto the PDMS substrate gives analytically the maximum scale width in terms of the post width $w_{post}$ and thickness $t_{post}$, scale bending stiffness $\overline{EI}_{scale}$, and scale/PDMS work of adhesion $\gamma$ .
(2) Eq. (5) [or Eq. (6)] based on the condition for scale contact gives analytically the minimal scale width in terms of the stretchability (maximum applied strain) $\varepsilon_{applied}$, bendability (minimum bending radius) $\rho$, post spacing $s_{post}$ and thickness $t_{post}$, and backing layer thickness $t_{backinglayer}$.
(3) Eq. (9) gives analytically the maximum strain in scale, which is linearly proportional to the ratio of scale thickness to bending radius, $t_{scale}/\rho$, and also depends on the applied strain, scale width, and post width and spacing via a single dimensionless parameter $\eta = (\varepsilon_{stretchability} - \varepsilon_{applied})s_{post}/(w_{scale} - w_{post})$. As shown in Eq. (10), the maximum strain in the scale has a simple upper bound of $3t_{scale}/(4\rho)$.

## Acknowledgments

The authors acknowledge support from NSF Grant Nos. ECCS-0824129 and OISE-1043143, and DOE, Division of Materials Sciences Grant No. DE-FG02-07ER46453.

## References

Crawford, G.P., 2005. Flexible Flat Panel Display Technology. Wiley, New York.
Forrest, S.R., 2004. The path to ubiquitous and low-cost organic electronic appliances on plastic. Nature 428, 911–918.
Gelinck, G.H., Huitema, H.E.A., Van Veenendaal, E., Cantatore, E., Schrijnemakers, L., Van der Putten, J., Geuns, T.C.T., Beenhakkers, M., Giesbers, J.B., Huisman, B.H., Meijer, E.J., Benito, E.M., Touwslager, F.J., Marsman, A.W., Van Rens, B.J.E., De Leeuw, D.M., 2004. Flexible active-matrix displays and shift registers based on solution-processed organic transistors. Nature Materials 3, 106–110.
Gere, J.M., Timoshenko, S.P., 2003. Mechanics of Materials: Solutions Manual. Nelson Thornes.
Jin, H.C., Abelson, J.R., Erhardt, M.K., Nuzzo, R.G., 2004. Soft lithographic fabrication of an image sensor array on a curved substrate. Journal of Vacuum Science & Technology B 22, 2548–2551.
Kim, D.H., Ahn, J.H., Choi, W.M., Kim, H.S., Kim, T.H., Song, J.Z., Huang, Y.G.Y., Liu, Z.J., Lu, C., Rogers, J.A., 2008a. Stretchable and foldable silicon integrated circuits. Science 320, 507–511.
Kim, D.H., Song, J., Choi, W.M., Kim, H.S., Kim, R.H., Liu, Z., Huang, Y.Y., Hwang, K.C., Zhang, Y.W., Rogers, J.A., 2008b. Materials and noncoplanar mesh designs for integrated circuits with linear elastic responses to extreme mechanical deformations. Proceedings of the National Academy of Sciences of the United States of America 105, 18675–18680.
Kim, D.H., Viventi, J., Amsden, J.J., Xiao, J.L., Vigeland, L., Kim, Y.S., Blanco, J.A., Panilaitis, B., Frechette, E.S., Contreras, D., Kaplan, D.L., Omenetto, F.G., Huang, Y.G., Hwang, K.C., Zakin, M.R., Litt, B., Rogers, J.A., 2010a. Dissolvable films of silk fibroin for ultrathin conformal bio-integrated electronics. Nature Materials 9, 511–517.
Kim, R.H., Kim, D.H., Xiao, J.L., Kim, B.H., Park, S.I., Panilaitis, B., Ghaffari, R., Yao, J.M., Li, M., Liu, Z.J., Malyarchuk, V., Kim, D.G., Le, A.P., Nuzzo, R.G., Kaplan, D.L., Omenetto, F.G., Huang, Y.G., Kang, Z., Rogers, J.A., 2010b. Waterproof AlInGaP optoelectronics on stretchable substrates with applications in biomedicine and robotics. Nature Materials 9, 929–937.
Kim, D.H., Lu, N.S., Ghaffari, R., Kim, Y.S., Lee, S.P., Xu, L.Z., Wu, J.A., Kim, R.H., Song, J.Z., Liu, Z.J., Viventi, J., de Graff, B., Elolampi, B., Mansour, M., Slepian, M.J., Hwang, S., Moss, J.D., Won, S.M., Huang, Y.G., Litt, B., Rogers, J.A., 2011a. Materials for multifunctional balloon catheters with capabilities in cardiac electrophysiological mapping and ablation therapy. Nature Materials 10, 316–323.
Kim, D.H., Lu, N.S., Ma, R., Kim, Y.S., Kim, R.H., Wang, S.D., Wu, J., Won, S.M., Tao, H., Islam, A., Yu, K.J., Kim, T.I., Chowdhury, R., Ying, M., Xu, L.Z., Li, M., Chung, H.J., Keum, H., McCormick, M., Liu, P., Zhang, Y.W., Omenetto, F.G., Huang, Y.G., Coleman, T., Rogers, J.A., 2011b. Epidermal Electronics. Science 333, 838–843.
Kim, S., Su, Y., Mihi, A., Lee, S., Liu, Z., Bhandakkar, T.K., Wu, J., Geddes III, J.B., Johnson, H.T., Zhang, Y., Park, J.-K., Braun, P.V., Huang, Y., Rogers, J.A., 2012. Imbricate scales as a design construct for microsystem technologies. Small 8, 901–906.
Ko, H.C., Stoykovich, M.P., Song, J.Z., Malyarchuk, V., Choi, W.M., Yu, C.J., Geddes, J.B., Xiao, J.L., Wang, S.D., Huang, Y.G., Rogers, J.A., 2008. A hemispherical electronic eye camera based on compressible silicon optoelectronics. Nature 454, 748–753.
Lumelsky, V.J., Shur, M.S., Wagner, S., 2001. Sensitive skin. Sensors Journal, IEEE 1, 41–51.
Mannsfeld, S.C.B., Tee, B.C.K., Stoltenberg, R.M., Chen, C.V.H.H., Barman, S., Muir, B.V.O., Sokolov, A.N., Reese, C., Bao, Z., 2010. Highly sensitive flexible pressure sensors with microstructured rubber dielectric layers. Nature Materials 9, 859–864.
Nathan, A., Park, B., Sazonov, A., Tao, S., Chan, I., Servati, P., Karim, K., Charania, T., Striakhilev, D., Ma, Q., Murthy, R.V.R., 2000. Amorphous silicon detector and thin film transistor technology for large-area imaging of X-rays. Microelectronics Journal 31, 883–891.
Park, S.I., Xiong, Y.J., Kim, R.H., Elvikis, P., Meitl, M., Kim, D.H., Wu, J., Yoon, J., Yu, C.J., Liu, Z.J., Huang, Y.G., Hwang, K., Ferreira, P., Li, X.L., Choquette, K., Rogers, J.A., 2009. Printed assemblies of inorganic light-emitting diodes for deformable and semitransparent displays. Science 325, 977–981.
Rogers, J.A., Someya, T., Huang, Y., 2010. Materials and mechanics for stretchable electronics. Science 327, 1603–1607.
Sekitani, T., Nakajima, H., Maeda, H., Fukushima, T., Aida, T., Hata, K., Someya, T., 2009. Stretchable active-matrix organic light-emitting diode display using printable elastic conductors. Nature Materials 8, 494–499.
Sekitani, T., Zschieschang, U., Klauk, H., Someya, T., 2010. Flexible organic transistors and circuits with extreme bending stability. Nature Materials 9, 1015–1022.
Someya, T., Sekitani, T., 2009. Printed skin-like large-area flexible sensors and actuators. In: Brugger, J., Briand, D. (Eds.), Proceedings of the Eurosensors Xxiii Conference. Elsevier Science Bv, Amsterdam, pp. 9–12.
Someya, T., Sekitani, T., Iba, S., Kato, Y., Kawaguchi, H., Sakurai, T., 2004. A large-area, flexible pressure sensor matrix with organic field-effect transistors for artificial skin applications. Proceedings of the National Academy of Sciences of the United States of America 101, 9966–9970.
Someya, T., Kato, Y., Sekitani, T., Iba, S., Noguchi, Y., Murase, Y., Kawaguchi, H., Sakurai, T., 2005. Conformable, flexible, large-area networks of pressure and thermal sensors with organic transistor active matrixes. Proceedings of the National Academy of Sciences of the United States of America 102, 12321–12325.
Song, J., Huang, Y., Xiao, J., Wang, S., Hwang, K.C., Ko, H.C., Kim, D.H., Stoykovich, M.P., Rogers, J.A., 2009. Mechanics of noncoplanar mesh design for stretchable electronic circuits. Journal of Applied Physics 105.
Su, Y., Wu, J., Fan, Z., Hwang, K.-C., Song, J., Huang, Y., Rogers, J.A., 2012. Postbuckling analysis and its application to stretchable electronics. Journal of the Mechanics and Physics of Solids 60, 487–508.

Viventi, J., Kim, D.-H., Moss, J.D., Kim, Y.-S., Blanco, J.A., Annetta, N., Hicks, A., Xiao, J., Huang, Y., Callans, D.J., Rogers, J.A., Litt, B., 2010. A conformal, bio-interfaced class of silicon electronics for mapping cardiac electrophysiology. Science Translational Medicine 2, 24ra22.

Viventi, J., Kim, D.H., Vigeland, L., Frechette, E.S., Blanco, J.A., Kim, Y.S., Avrin, A.E., Tiruvadi, V.R., Hwang, S.W., Vanleer, A.C., Wulsin, D.F., Davis, K., Gelber, C.E., Palmer, L., Van der Spiegel, J., Wu, J., Xiao, J., Huang, Y., Contreras, D., Rogers, J.A., Litt, B., 2011. Flexible, foldable, actively multiplexed, high-density electrode array for mapping brain activity in vivo. Nature Neuroscience 14, 1599–1605.

Yoon, J., Baca, A.J., Park, S.I., Elvikis, P., Geddes, J.B., Li, L.F., Kim, R.H., Xiao, J.L., Wang, S.D., Kim, T.H., Motala, M.J., Ahn, B.Y., Duoss, E.B., Lewis, J.A., Nuzzo, R.G., Ferreira, P.M., Huang, Y.G., Rockett, A., Rogers, J.A., 2008. Ultrathin silicon solar microcells for semitransparent, mechanically flexible and microconcentrator module designs. Nature Materials 7, 907–915.